Letters

An Online Power Angle Remote Estimation Method for GFL-GFM-Converters Paralleled System

Zhen Tian, *Member, IEEE*, Pan Feng, Xilin Li, *Graduate Student Member, IEEE*, Meng Huang, *Member, IEEE*, Behrooz Bahrani, *Senior Member, IEEE*, Xiaoming Zha, *Senior Member, IEEE*, and Chong Shao

***Abstract*—Complicated dynamic interactions in multi-grid-connected converter (GCC) systems have unexpected impacts on the overall response of the system. Online state sharing among different GCCs can enhance the coordination of the whole system. However, due to the significant communication delay, the power angle and frequency states cannot be transmitted rapidly enough. In this letter, an innovative power angle remote estimation method is proposed to realize real-time power angle and frequency information sharing among different GCCs with the local measurement of voltage and power. This method decouples interactive information by revealing the transient response mechanism of the network. The proposed method could inspire distributed cooperative control and online transient stability analysis for multi-GCC systems.**

***Index Terms*—Distributed cooperative control, grid-connected converters (GCCs), microgrid (MG), online power angle estimation, transient stability.**

I. Introduction

GRID-CONNECTED converters (GCCs) are widely utilized to integrate renewable energy sources. GCCs can be divided into two categories: grid-following converters (GFLCs) [1] and grid-forming converters (GFMCs) [2]. However, both of them are designed based on the single-machine infinite-bus system and fail to account for the complicated dynamic interactions in the multi-GCC paralleled system (MCPS) [3]. These undesired coupling interactions in the MCPS compromise system stability and are hard to quantify since they are path dependent. Access to each other's transient power angles is essential for implementing cooperative transient control and online stability assessment in the MCPS. Existing cooperative control primarily relies on communication, but its delay is as high as 200 ms [4], which is impractical for the GFLC. This communication delay is mainly due to the communication protocol. The online estimation method has been widely applied in impedance estimation but has not been adopted to power angle and frequency estimation yet [5]. In practice, even the converters' own transient power angles are unknown, since the grid frequency change during a fault is unpredictable. This lack of knowledge prevents online stability assessment, even if stability region estimation is available [6].

In this letter, an online estimation method of both the local and remote GCCs' power angle–frequency information is proposed for a GFLC–GFMC paralleled system, commonly utilized in offshore wind power plants (OWPPs) paralleled with onshore battery energy storage systems (BESSs) [7]. This letter reveals transient dynamic response mechanisms of the network and enables decouple of interactive information from the physical quantities measured locally by each GCC. Consequently, each GCC can access its own power angle and that of the other converter within a millisecond scale, which is significant faster than the traditional communication method. As it requires no additional equipment, the proposed method is more economical and reliable than communication-based methods.

The proposed noncommunication state sharing among GCCs could promote the research on transient cooperative control and online transient stability assessment for the MCPS. It is important to note that the proposed online estimation method primarily relies on the network mechanism, making it versatile across all the control types. Based on the observed states, an example of transient cooperative control is presented in Section IV to illustrate the practical application of the proposed method.

II. System Modeling

The structure of the GFMC–GFLC paralleled system is given in Fig. 1. The GFLC and the GFMC are paralleled at S through lines $\boldsymbol{Z}_{\mathbf{GFL}}$ and $\boldsymbol{Z}_{\mathbf{GFM}}$ and together connected to the grid

Manuscript received 29 March 2024; revised 6 May 2024; accepted 14 May 2024. Date of publication 17 May 2024; date of current version 4 September 2024. This work was supported in part by the National Key Research and Development Program of China under Grant 2022YFB2402700 and in part by the Science and Technology Project of State Grid Corporation of China under Grant 52272222001J. *(Corresponding author: Xilin Li.)*

Zhen Tian, Pan Feng, Xilin Li, Meng Huang, and Xiaoming Zha are with the Hubei Key Laboratory of Power Equipment and System Security for Integrated Energy, School of Electrical Engineering and Automation, Wuhan University, Wuhan 430072, China (e-mail: ztian.ee@whu.edu.cn; 2023202070069@whu.edu.cn; snplee@whu.edu.cn; meng.huang@whu.edu.cn; xmzha@whu.edu.cn).

Behrooz Bahrani is with the Department of Electrical and Computer Systems Engineering, Monash University, Clayton, VIC 3800, Australia (e-mail: behrooz.bahrani@monash.edu).

Chong Shao is with the State Grid Gansu Electric Power Company, Lanzhou 730046, China (e-mail: shaochong@gs.sgcc.com.cn).

Color versions of one or more figures in this article are available at https://doi.org/10.1109/TPEL.2024.3402228.

Digital Object Identifier 10.1109/TPEL.2024.3402228

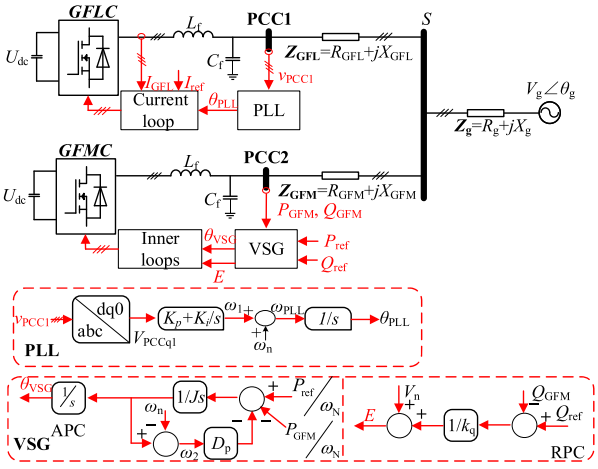

Fig. 1. Structure and the controller of the GFMC–GFLC paralleled system.

through $\boldsymbol{Z}_g$. V_g and θ_g are the amplitude and phase of the grid voltage, respectively. L_f and C_f are the inductance and capacitance of the output filter, respectively. In practice, the OWPP adopts the GFLC, while the accompanying onshore BESS uses the GFMC. Therefore, $\boldsymbol{Z}_{\mathbf{GFL}}$ is larger than $\boldsymbol{Z}_{\mathbf{GFM}}$.

GFLC's control includes a phase-locked loop (PLL) and a current loop. K_p and K_i are PLL's proportional and integral coefficients, respectively. θ_{PLL} and ω_{PLL} are PLL's output phase and frequency, respectively, while ω_n is the nominal frequency. The dynamics of the current loop are much faster than those of the PLL and can be ignored when analyzing transient stability. Therefore, GFLC's output current $\boldsymbol{I}_{\mathbf{GFL}}$ can be assumed to equal the current reference: $\boldsymbol{I}_{\mathbf{GFL}} = \boldsymbol{I}_{\mathbf{ref}} = \boldsymbol{I}_{\mathbf{ref}}\angle\varphi_I = \boldsymbol{I}_{\mathbf{ref}d} + j\boldsymbol{I}_{\mathrm{ref}q}$. $\varphi_I = \tan^{-1}(\boldsymbol{I}_{\mathrm{ref}q}/\boldsymbol{I}_{\mathrm{ref}d})$ is defined as the power factor angle of the GFLC. GFMC's control utilizes the virtual synchronous generator (VSG) as the active power controller (APC), and it includes a droop-based reactive power controller (RPC).

In addition, GFMC's control includes voltage and current inner loops. The dynamics of inner loops are much faster than those of the VSG and, thus, are also ignored. The output voltage of the GFMC is assumed to be $E\angle\theta_{\mathrm{VSG}}$, where E and θ_{VSG} are the output voltage amplitude and phase of APC and RPC, respectively. J and D_P are the virtual inertia and damping of APC, respectively. P_{ref} and Q_{ref} are active and reactive power references of the VSG, respectively. k_q and V_n are the proportional coefficient and nominal voltage of the RPC, respectively. P_{GFM} and Q_{GFM} are the output active power and reactive power of the GFMC, respectively. Based on the nodal analysis method, it can be derived that

$$\begin{bmatrix} \boldsymbol{Y}_{\mathbf{GFM}}+\boldsymbol{Y}_{\boldsymbol{g}} & -\boldsymbol{Y}_{\mathbf{GFM}} & -\boldsymbol{Y}_{\boldsymbol{g}} \\ -\boldsymbol{Y}_{\mathbf{GFM}} & \boldsymbol{Y}_{\mathbf{GFM}} & 0 \\ -\boldsymbol{Y}_{\boldsymbol{g}} & 0 & \boldsymbol{Y}_{\boldsymbol{g}} \end{bmatrix} \begin{bmatrix} \boldsymbol{V}_S \\ \boldsymbol{E} \\ \boldsymbol{V}_{\boldsymbol{g}} \end{bmatrix} = \begin{bmatrix} \boldsymbol{I}_{\mathbf{GFL}} \\ \boldsymbol{I}_{\mathbf{GFM}} \\ \boldsymbol{I}_{\mathbf{g}} \end{bmatrix} \tag{1}$$

where $\boldsymbol{Y}_i = 1/\boldsymbol{Z}_i$ are the admittances of $\boldsymbol{Z}_i$. $\boldsymbol{I}_{\mathrm{GFM}}$ and $\boldsymbol{I}_g$ are the current on $\boldsymbol{Z}_{\mathbf{GFM}}$ and Z_g, respectively. $\boldsymbol{V}_S$ is the voltage at S. The power angles of the paralleled system can be defined as follows:

$$\delta_1 = \theta_{\mathrm{PLL}} - \theta_g, \quad \delta_2 = \theta_{\mathrm{VSG}} - \theta_g, \quad \delta_{21} = \theta_{\mathrm{VSG}} - \theta_{\mathrm{PLL}}. \tag{2}$$

The PCC1's voltage $\boldsymbol{v}_{\mathrm{PCC1}}$ can be derived as

$$\boldsymbol{v}_{\mathbf{PCC1}} = \boldsymbol{Z}_{\mathbf{GFL}}\boldsymbol{I}_{\mathbf{ref}} + \boldsymbol{V}_{\mathrm{S}}. \tag{3}$$

Applying park transformation on $\boldsymbol{v}_{\mathrm{PCC1}}$ with θ_{PLL}, the dq-axis components $V_{\mathrm{PCC1}\,d}$ and $V_{\mathrm{PCC1}\,q}$ can be derived based on (1)–(3)

$$\begin{aligned} V_{\mathrm{PCC1}d} &= \underbrace{I_{\mathrm{ref}}a_1\cos(\varphi_I+\theta_1) + I_{\mathrm{ref}}a_4\cos(\varphi_I+\theta_4)}_{C_d} \\ &\quad + a_2E\cos(\delta_{21}+\theta_2) + a_3V_{\mathrm{g}}\cos(\delta_1-\theta_3) \\ V_{\mathrm{PCC1}q} &= \underbrace{I_{\mathrm{ref}}a_1\sin(\varphi_I+\theta_1) + I_{\mathrm{ref}}a_4\sin(\varphi_I+\theta_4)}_{C_q} \\ &\quad + a_2E\sin(\delta_{21}+\theta_2) - a_3V_{\mathrm{g}}\sin(\delta_1-\theta_3). \end{aligned} \tag{4}$$

The coefficients a_1–a_4 and θ_1–θ_4 are denoted as follows:

$$\begin{aligned} a_1\angle\theta_1 &= 1/(\boldsymbol{Y}_{\mathbf{GFM}}+\boldsymbol{Y}_{\mathbf{g}}), \quad a_2\angle\theta_2 \\ &= \boldsymbol{Y}_{\mathbf{GFM}}/(\boldsymbol{Y}_{\mathbf{GFM}}+\boldsymbol{Y}_{\mathbf{g}}) \\ a_3\angle\theta_3 &= \boldsymbol{Y}_{\mathbf{g}}/(\boldsymbol{Y}_{\mathbf{GFM}}+\boldsymbol{Y}_{\mathbf{g}}), \quad a_4\angle\theta_4 = 1/(\boldsymbol{Y}_{\mathbf{GFL}}). \end{aligned} \tag{5}$$

Combining (1) and (2), P_{GFM} and Q_{GFM} can be derived as

$$\begin{aligned} P_{\mathrm{GFM}} &= 1.5\left[E^2G_5 - EV_ga_5\cos(\delta_2-\theta_5)\right. \\ &\quad \left. - EI_{\mathrm{ref}}a_2\cos(\delta_{21}-\theta_2-\varphi_{\mathrm{I}})\right] \\ Q_{\mathrm{GFM}} &= -1.5\left[E^2B_5 + EV_ga_5\sin(\delta_2-\theta_5)\right. \\ &\quad \left. + EI_{\mathrm{ref}}a_2\sin(\delta_{21}-\theta_2-\varphi_{\mathrm{I}})\right] \end{aligned} \tag{6}$$

where a_5 and θ_5 are denoted as follows:

$$a_5\angle\theta_5 = \boldsymbol{Y}_{\mathbf{GFM}}\boldsymbol{Y}_g/(\boldsymbol{Y}_{\mathbf{GFM}}+\boldsymbol{Y}_{\mathbf{g}}) = G_5 + jB_5. \tag{7}$$

According to the controller structure in Fig. 1, the dynamics of the PLL and the VSG can be denoted as

$$\ddot{\delta}_1 = K_iV_{\mathrm{PCC}q1} + K_p\dot{V}_{\mathrm{PCC}q1} \tag{8}$$

$$\begin{cases} J\ddot{\delta}_2 = P_{\mathrm{ref}}/\omega_n - P_{\mathrm{GFM}}/\omega_n - D_p\dot{\delta}_2 \\ E = V_n + (Q_{\mathrm{ref}} - Q_{\mathrm{GFM}})/k_q. \end{cases} \tag{9}$$

Combining (6) and (9) can obtain the RPC's output voltage E

$$E(\delta_2,\delta_1) = \left[-q_2(\delta_2,\delta_1) + \sqrt{q_2^2(\delta_2,\delta_1) - 4q_1q_3}\right] \Big/ 2q_1 \tag{10}$$

where constants q_1 and q_3 and function $q_2(\delta_1, \delta_2)$ are derived as

$$\begin{aligned} q_1 &= 1.5B_5, \quad q_3 = Q_{\mathrm{ref}} + k_qV_n \\ q_2 &= 1.5\left(V_ga_5\sin(\delta_2-\theta_5) + I_{\mathrm{ref}}a_2\sin(\delta_{21}-\theta_2-\varphi_{\mathrm{I}})\right) - k_q. \end{aligned} \tag{11}$$

As shown in (4), (6), and (8)–(11), the transient dynamics of the GFLC and the GFMC are strongly coupled with each other. This causes cascade synchronous instability, which brings a serious challenge to systems' safe operation. The distances

between the OWPP and the BESS are usually very far. Thus, it is unrealistic for the local GCC to access the states of the remote GCC through communication. Due to the physical connection of lines, each converter's locally measured physical quantities contain the power angle information of the other converter. This letter reveals the transient interaction mechanism of the MCPS under large disturbances and proposes an estimation method to realize online estimation of both the local and remote GCCs' power angles and frequencies based on the locally measured physical quantities.

III. Online State Estimation Algorithm

In this section, both the remote and local GCCs' power angles during normal operation and after fault clearance are accurately and quickly estimated based on the locally detected physical quantities: $V_{\mathrm{PCC1}\,d}$ and $V_{\mathrm{PCC1}\,q}$ for the GFLC and P_{GFM} and Q_{GFM} for the GFMC. Note that the local power angle cannot be directly integrated with the predisturbance equilibrium as the initial conditions, because the change in grid frequency during the fault remains unknown. Therefore, this section also explains how to estimate the local power angle.

A. State Estimation Method for the GFLC

For the initial time t_0, which is identified as when the converter detects the fault is cleared, the calculated values ${\delta^0}_{\mathrm{1ca}}$, ${\delta^0}_{\mathrm{2ca}}$, and ${E^\circ}_{\mathrm{ca}}$ (the subscript "ca" represents the calculated value by the proposed method, and the superscript represents in which time this value exists) can be derived based on the measured ${V^0}_{\mathrm{PCC1}\,d}$ and ${V^0}_{\mathrm{PCC1}\,q}$

$$\delta^0_{2\mathrm{ca}}=\cos^{-1}\left(\begin{matrix}\left(V^0_{\mathrm{PCC1}d}-C_d\right)^2-\left(a_2E^0_{\mathrm{ca}}\right)^2\\+\left(V^0_{\mathrm{PCC1}q}-C_q\right)^2-\left(a_3V_g\right)^2\end{matrix}\Big/\,2a_2a_3EV_g\right)+\theta_3-\theta_2 \tag{12}$$

$$\begin{cases}\delta^0_{1\mathrm{ca}}=\cos^{-1}\dfrac{V^0_{\mathrm{PCC1}d}-C_d}{\sqrt{\begin{matrix}\left[a_3V_g\cos\theta_3+a_2E^0_{\mathrm{ca}}\cos(\delta^0_{2\mathrm{ca}}+\theta_2)\right]^2\\+\left[a_3V_g\sin\theta_3+a_2E^0_{\mathrm{ca}}\sin(\delta^0_{2\mathrm{ca}}+\theta_2)\right]^2\end{matrix}}}+\gamma^0\\ \gamma^0=tan^{-1}\dfrac{a_3V_g\sin\theta_3+a_2E^0_{\mathrm{ca}}\sin(\delta^0_{2\mathrm{ca}}+\theta_2)}{a_3V_g\cos\theta_3+a_2E^0_{\mathrm{ca}}\cos(\delta^0_{2\mathrm{ca}}+\theta_2)}\end{cases} \tag{13}$$

$$E^0_{\mathrm{ca}}=\left(-q_2\left(\delta^0_{2\mathrm{ca}},\delta^0_{1\mathrm{ca}}\right)+\sqrt{q_2^2\left(\delta^0_{2\mathrm{ca}},\delta^0_{1\mathrm{ca}}\right)-4q_1q_3}\right)\Big/\,2q_1. \tag{14}$$

The specific expression of C_{d} and C_{q} can be found in (4). Equation (12) is derived by moving the C_d and C_q terms to the left of (4) and then summing the squares of ${V^0}_{\mathrm{PCC1}\,d}$–C_d and ${V^0}_{\mathrm{PCC1}\,q}$–C_q. Terms relating to δ_1 can be cleverly eliminated by trigonometric function identity transformation. Equation (13) is derived by decoupling the δ_1 terms in the expression of V_{PCC1d} (4), and (14) is derived based on (10) and (11). Equations (12)–(14) are ternary nonlinear algebraic equations of ${\delta^0}_{\mathrm{1ca}}$, ${\delta^0}_{\mathrm{2ca}}$, and ${E^\circ}_{\mathrm{ca}}$, respectively, which can converge by about two

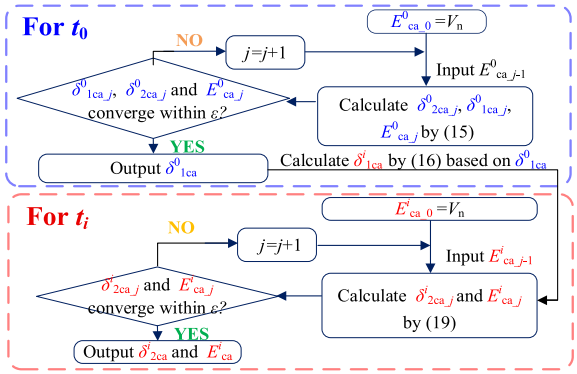

Fig. 2. Iterative process of the GFLC's estimation algorithm.

to three times of iterations

$$\begin{cases}E^0_{\mathrm{ca\_0}}=V_n,\quad \delta^0_{2\mathrm{ca}\_j}=f_{12}\left(E^0_{\mathrm{ca}\_j-1}\right)\\ \delta^0_{1\mathrm{ca}\_j}=f_{13}\left(\delta^0_{2\mathrm{ca}\_j},E^0_{\mathrm{ca}\_j-1}\right),\quad E^0_{\mathrm{ca}\_j}=f_{14}\left(\delta^0_{1\mathrm{ca}\_j},\delta^0_{2\mathrm{ca}\_j}\right)\end{cases} \tag{15}$$

where the parameter ${x^0}_j$ represents the result of the jth iteration at time t_0, and functions f_{12}, f_{13}, and f_{14} refer to the formulas (12)–(14), respectively. The selection of t_0 does not have much effect on the proposed estimation method, since the iterations at each time t_i are independent. Based on the measured ${V^i}_{\mathrm{PCC1d}}$ and ${V^i}_{\mathrm{PCC1q}}$ at time t_i, ${\delta^i}_{\mathrm{1ca}}$, ${\delta^i}_{\mathrm{2ca}}$, and ${E^i}_{\mathrm{ca}}$ are derived as follows:

$$\delta^i_{1\mathrm{ca}}=\delta^0_{1\mathrm{ca}}+\int_{t_0}^{t_i}\omega_1dt \tag{16}$$

$$\delta^i_{2\mathrm{ca}}=\cos^{-1}\left(\begin{matrix}\left(V^i_{\mathrm{PCC1}d}-C_d\right)^2-\left(a_2E^i_{\mathrm{ca}}\right)^2\\+\left(V^i_{\mathrm{PCC1}q}-C_q\right)^2-\left(a_3V_g\right)^2\end{matrix}\Big/\,2a_2a_3E^i_{\mathrm{ca}}V_g\right)+\theta_3-\theta_2 \tag{17}$$

$$E^i_{\mathrm{ca}}=\left(-q_2\left(\delta^i_{2\mathrm{ca}},\delta^i_{1\mathrm{ca}}\right)+\sqrt{q_2^2\left(\delta^i_{2\mathrm{ca}},\delta^i_{1\mathrm{ca}}\right)-4q_1q_3}\right)\Big/\,2q_1 \tag{18}$$

where ω_1 is the frequency of δ_1, which is a directly available value for the GFLC. Equations (17) and (18) are binary nonlinear algebraic equations concerning ${\delta^i}_{\mathrm{2ca}}$ and ${E^i}_{\mathrm{ca}}$, which can converge by about two to three times of iterations in the following equation:

$$\begin{aligned}E^i_{\mathrm{ca\_0}}=V_n,\quad \delta^i_{2\mathrm{ca}\_j}&=f_{17}\left(E^i_{\mathrm{ca}\_j-1}\right),\quad E^i_{\mathrm{ca}\_j}\\&=f_{18}\left(\delta^i_{1\mathrm{ca}},\delta^i_{2\mathrm{ca}\_j}\right)\end{aligned} \tag{19}$$

where the parameter ${x^i}_j$ represents the result of the jth iteration at time t_i, and functions f_{18} and f_{19} refer to the formulas (18) and (19), respectively.

The frequency ${\omega^i}_{\mathrm{2ca}}$ of GFMC's power angle can be derived by differentiating the calculated ${\delta^i}_{\mathrm{2ca}}$

$$\omega^i_{2\mathrm{ca}}=\left(\delta^i_{2\mathrm{ca}}-\delta^{i-1}_{2\mathrm{ca}}\right)/(t_i-t_{i-1}). \tag{20}$$

The overall flowchart of the GFLC online state estimation algorithm is summarized in Fig. 2. It is seen that the iteration at time t_0 is calculated by (15), while the iteration at $\forall t_i$ is

calculated by (19). Iterations at different times t_i do not affect each other. Test results show that both (15) and (19) can converge after only two to three iterations and cost about 10 μs. In other words, the proposed iterative method can realize online monitoring of other converters' power angle and voltage with almost no delay, while the communication equipment fails.

B. State Estimation Method for the GFMC

Similarly, the GFMC can also calculate the power angle ${\delta^i}_{1\mathrm{ca}}$ of the GFLC by measuring its own output ${P^i}_{\mathrm{GFM}}$ and ${Q^i}_{\mathrm{GFM}}$

$$\delta^i_{1\mathrm{ca}} = \cos^{-1}\left[\begin{array}{l}\left(2P^i_{\mathrm{GFM}}/3-\left(E^i\right)^2G_5\right)^2\\ -\left(E^i\right)^2V_g^2a_5^2-\left(E^i\right)^2I_{\mathrm{ref}}^2a_2^2\\ +\left(2Q^i_{\mathrm{GFM}}/3+\left(E^i\right)^2B_5\right)^2\end{array}\Big/\,2\left(E^i\right)^2V_gI_{\mathrm{ref}}a_5a_2\right]+\theta_5-\theta_2-\varphi_{\mathrm{I}}. \tag{21}$$

Equation (21) is derived by trigonometric function identity transformation over (6). Terms relating to δ_2 can be neatly eliminated. The frequency ${\omega^i}_{1\mathrm{ca}}$ of GFLC's power angle can be derived by differentiating the calculated ${\delta^i}_{1\mathrm{ca}}$

$$\omega^i_{1\mathrm{ca}} = \left(\delta^i_{1\mathrm{ca}}-\delta^{i-1}_{1\mathrm{ca}}\right)/(t_i-t_{i-1}). \tag{22}$$

Based on ${\delta^0}_{1\mathrm{ca}}$ derived in (21), ${\delta^0}_{2\mathrm{ca}}$ at t_0 can be obtained by combining the active power expression in (6)

$$\delta^0_{2\mathrm{ca}} = \cos^{-1}\left[\left(\left(E^0\right)^2G_5-2P^0_{\mathrm{GFM}}/3\right)\Big/\sqrt{a_6^2+a_7^2}\right]+\theta_8 \tag{23}$$

where coefficients a_6, a_7, and θ_8 are denoted as follows:

$$\begin{aligned}a_6 &= E^0V_ga_5\cos\theta_5+E^0I_{\mathrm{ref}}a_2\cos\left(\delta^0_{1\mathrm{ca}}+\theta_2+\varphi_{\mathrm{I}}\right)\\ a_7 &= E^0V_ga_5\sin\theta_5+E^0I_{\mathrm{ref}}a_2\sin\left(\delta^0_{1\mathrm{ca}}+\theta_2+\varphi_{\mathrm{I}}\right)\\ \theta_8 &= \tan^{-1}\left(a_7/a_6\right).\end{aligned} \tag{24}$$

For $\forall$ time t_i, the corresponding ${\delta^i}_{2\mathrm{ca}}$ can be derived as

$$\delta^i_{2\mathrm{ca}} = \delta^0_{2\mathrm{ca}}+\int_{t_0}^{t_i}\omega_2dt \tag{25}$$

where ω_2 is the frequency of δ_2, which is a directly available value for the GFMC. The state estimation algorithm for the GFMC, shown in (21)–(25), does not need iteration. This is because the RPC's output voltage E^i is available to the GFMC. Since the proposed algorithm is analytic algebraic operation and does not require iteration, it is significantly faster than communication.

IV. Verification and Application Demonstration of the Proposed Method

The online state estimation method proposed in the previous section realizes real-time state sharing among GCCs, which facilitates coordinated control strategies and online stability monitoring methods for multi-GCC systems. The parameters of the system adopted for the verification of the proposed approach are listed as follows: $V_{\mathrm{g}} = V_{\mathrm{n}} = 311$ V, $R_{\mathrm{GFL}} = 0.1\ \Omega$, $L_{\mathrm{GFL}} = 1$ mH, $R_{\mathrm{GFM}} = 0.05\ \Omega$, $L_{\mathrm{GFM}} = 0.5$ mH, $R_g = 0.15\ \Omega$, $L_{\mathrm{g}} = 1.5$ mH, $\omega_n = 100\,\pi$, $\boldsymbol{I}_{\mathrm{ref}} = 250$ A, $\varphi_I = 0.02$, $K_p = 0.07$, $K_i = 10$, $P_{\mathrm{ref}} = 170$ kW, $J = 10$, $D_p = 15$, $Q_{\mathrm{ref}} = 20$ kVar, and $K_q = 10^5$.

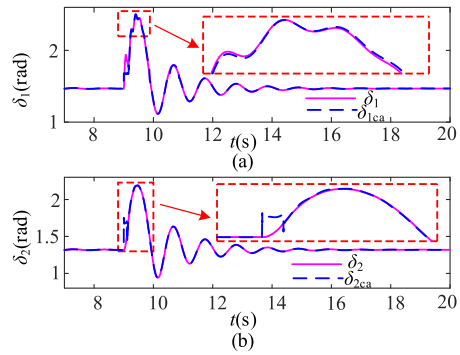

Fig. 3. (a) and (b) Time-domain comparison of $\delta_{1\mathrm{ca}}$ and $\delta_{2\mathrm{ca}}$ with δ_1 and δ_2, respectively.

TABLE I
Error Effects of Parameter Drift on Accuracy

Parameter drift	$\delta_{1\mathrm{ca}}$ by GFMC	$\delta_{2\mathrm{ca}}$ by GFLC
1.01 p.u./ 0.99 p.u. V_{g}	0.79%/–0.97%	0.39%/–0.48%
1.01 p.u./ 0.99 p.u. $\boldsymbol{Z}_{\mathrm{g}}$	0.34%/–0.67%	0.23%/–0.31%
1.01 p.u./ 0.99 p.u. $\boldsymbol{Z}_{\mathrm{GFL}}$	0.13%/–0.35%	–0.34%/0.26%
1.01 p.u./ 0.99 p.u. $\boldsymbol{Z}_{\mathrm{GFM}}$	0.12%/–0.38%	–0.41%/0.34%
No parameter drift	–0.13%	–0.04%

A. Accuracy Verification of the Proposed Estimation Method

The time-domain verification of the proposed state estimation method is illustrated in Fig. 3. The grid voltage amplitude drops to 0.3 p.u. at 9 s and recovers to 1 p.u. at 9.12 s. The GFLC's power angle estimation $\delta_{1\mathrm{ca}}$ calculated by the GFMC and the GFMC's power angle estimation $\delta_{2\mathrm{ca}}$ calculated by the GFLC are the blue dashed curves in Fig. 3(a) and (b), respectively. The simulation results of GFLC's phase difference δ_1 with grid and GFMC's phase difference δ_2 with grid are the pink solid curves in Fig. 3(a) and (b), respectively. The calculated values $\delta_{1\mathrm{ca}}$ and $\delta_{2\mathrm{ca}}$ demonstrate little error compared to the actual values δ_1 and δ_2 during the transient process. It is important to note that the errors are relatively significant at 9–9.12 s, since the system parameters under fault (i.e., the voltage dip degree) are unknown to GCCs. However, considering that the stability analysis and cooperative control are mostly aimed at the system after fault removal, these large errors in 9–9.12 s do not affect the effectiveness of the proposed online power angle estimation method.

Table I shows the average errors of the proposed method within 5 s (disturbance is the same as Fig. 3) under different parameter drifts, indicating that it is robust against parameter variations and offers a significant practical value.

B. Application Demonstration

To exhibit the practicality of the proposed online estimation method, a cooperative control without communication is given as an example in this section. Applying the online estimation

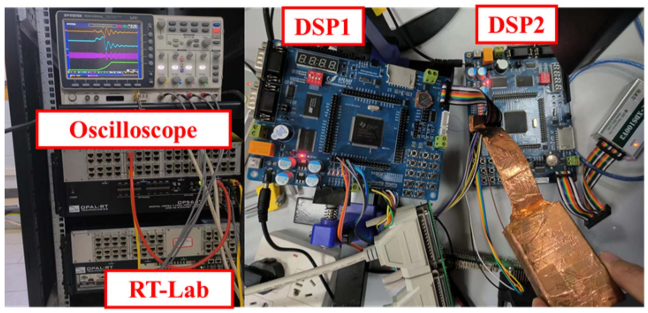

Fig. 4. Hardware-in-the-loop experimental platform.

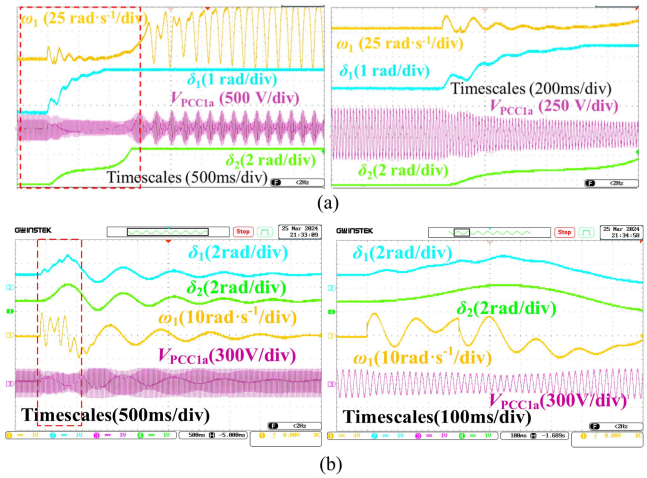

Fig. 5. Experimental verification of the proposed stability enhanced control. (a) Unstable when fault recovers at 120 ms, without the proposed control. (b) Stable when fault recovers at 300 ms, with the proposed control.

method, each GCC in the system shown in Fig. 1 can sense the power angle–frequency real-time values of the local and remote GCCs with almost no delay. This yields that the GCCs can realize the active online estimation of the complicated interactions among different GCCs.

When the GCCs detect that the interaction terms at a certain time are unfavorable to their own transient stability, the compensation for undesired interaction terms' effects will be conducted. Specific control strategies of the GFLC and the GFMC are given as follows:

$$\begin{aligned}\theta_{\text{PLL}} =& \int \left[\omega_n + K_i \int \left(F_{\text{GFL}} + V_{\text{PCC}q1}\right) dt \right. \\ &\left. + K_p \left(F_{\text{GFL}} + V_{\text{PCC}q1}\right)\right] dt \\ F_{\text{GFL}} =& -a_2 E_{\text{ca}} \sin\left(\delta_{21\text{ca}} + \theta_2\right) \text{when} \sin\left(\delta_{21\text{ca}} + \theta_2\right) > 0 \\ F_{\text{GFL}} =& \, 0 \,\text{when}\, \sin\left(\delta_{21\text{ca}} + \theta_2\right) \le 0 \end{aligned} \tag{26}$$

$$\begin{aligned} J\ddot{\theta}_{\text{VSG}} =& P_{\text{ref}}/\omega_n - \left(P_{\text{GFM}} + 1.5F_{\text{GFM}}a_2E\right)/\omega_n \\ &- D_p\left(\dot{\theta}_{\text{VSG}} - \omega_n\right) \\ F_{\text{GFM}} =& I_{\text{ref}} \cos\left(\delta_{21\text{ca}} - \theta_2 - \varphi_{\text{I}}\right) \text{when} \cos\left(\delta_{21\text{ca}}\right. \\ &\left. - \theta_2 - \varphi_I\right) > 0 \\ F_{\text{GFM}} =& \, 0 \,\text{when}\, \cos\left(\delta_{21\text{ca}} - \theta_2 - \varphi_I\right) < 0. \end{aligned} \tag{27}$$

As shown in Fig. 4, an RT-Lab-based hardware-in-the-loop experimental platform is built to verify the proposed cooperative control. Without cooperative control, the system loses stability when the grid voltage drops to 0.2 p.u. and recovers at 120 ms, as shown in Fig. 5(a). However, with the proposed control, the system can still maintain stability under the same voltage dip, even if the fault recovery time increases to 300 ms, as shown in Fig. 5(b).

V. Conclusion

This letter introduces an online state estimation method for the GFLC–GFMC paralleled system. By elucidating the system's transient dynamic response mechanism, the proposed method facilitates real-time power angle sharing among different converters within milliseconds—significantly faster than conventional communication equipment. This method promotes enhanced transient stability and cooperative control, as well as online stability assessments for multiconverter systems. An example application of a stability-enhanced cooperative control strategy is provided to demonstrate the effectiveness and practicability of this estimation method. It is important to note that the proposed method primarily based on the network mechanism is adaptable to various system structures; the GFLC–GFMC system discussed in this letter serves merely as one example.

References

[1] Y. Zhang, C. Zhang, and X. Cai, "Large-signal grid-synchronization stability analysis of PLL-based VSCs using Lyapunov's direct method," *IEEE Trans. Power Syst.*, vol. 37, no. 1, pp. 788–791, Jan. 2022.

[2] X. He, S. Pan, and H. Geng, "Transient stability of hybrid power systems dominated by different types of grid-forming devices," *IEEE Trans. Energy Convers.*, vol. 37, no. 2, pp. 868–879, Jun. 2022.

[3] X. He and H. Geng, "PLL synchronization stability of grid-connected multi converter systems," *IEEE Trans. Ind. Appl.*, vol. 58, no. 1, pp. 830–842, Jan./Feb. 2022.

[4] O. Shafiee, J. M. Guerrero, and J. C. Vasquez, "Distributed secondary control for islanded microgrids—A novel approach," *IEEE Trans. Power Electron.*, vol. 29, no. 2, pp. 1018–1031, Feb. 2014.

[5] J. Sun, J. Yu, J. Qiu, and Y. Wang, "Transient responses based grid impedance estimation for grid-forming converters," in *Proc. 4th Int. Conf. Elect. Eng. Control Technol.*, 2022, pp. 741–745.

[6] X. Li et al., "Nonlinear modeling and stability analysis of grid-tied paralleled-converters systems based on the proposed dual-iterative equal area criterion," *IEEE Trans. Power Electron.*, vol. 38, no. 6, pp. 7746–7759, Jun. 2023.

[7] F. Zhao et al., "Control interaction modeling and analysis of grid-forming battery energy storage system for offshore wind power plant," *IEEE Trans. Power Syst.*, vol. 37, no. 1, pp. 497–507, Jan. 2022.